Applied Catalysis B: Environmental 184 (2016) 264–269

Contents lists available at ScienceDirect

Applied Catalysis B: Environmental

journal homepage: www.elsevier.com/locate/apcatb

Solvent-induced deposition of Cu–Ga–In–S nanocrystals onto a titanium dioxide surface for visible-light-driven photocatalytic hydrogen production

Tarek A. Kandiel[a,b,**], Kazuhiro Takanabe[a,*]

[a] Division of Physical Sciences and Engineering, KAUST Catalysis Center (KCC), King Abdullah University of Science and Technology (KAUST), Thuwal 23955-6900, Saudi Arabia
[b] Department of Chemistry, Faculty of Science, Sohag University, Sohag 82524, Egypt

ARTICLE INFO

Article history:
Received 6 October 2015
Received in revised form
15 November 2015
Accepted 22 November 2015
Available online 25 November 2015

Keywords:
Quaternary nanocrystals
Photocatalysis
CGIS
Hydrogen production
Titanium dioxide

ABSTRACT

In this paper, copper–gallium–indium–sulfide (CGIS) nanocrystals with different Ga/In ratios, i.e., $CuGa_xIn_{5-x}S_8$, where $x = 0–5$, were synthesized and investigated for visible-light-driven hydrogen (H_2) evolution from aqueous solutions that contain sulfide/sulfite ions. The synthesized CGIS nanocrystals were characterized by diffuse reflectance spectroscopy (DRS), X-ray diffraction (XRD), transmission electron microscopy (TEM), and photoluminescence spectroscopy (PL). With 1.0 wt.% Ru as a co-catalyst, the H_2 evolution rate on $CuGa_2In_3S_8$ (CGIS hereafter) showed the highest activity. The CGIS nanocrystals were deposited onto a TiO_2 surface via a unique solvent-induced deposition method. The CGIS/TiO_2 photocatalyst showed comparable activity to that obtained using bare CGIS nanocrystals when the photocatalyst amount was sufficient in the photoreactor system, suggesting that TiO_2 remains intact in terms of photocatalytic activity. The quantity of CGIS nanocrystals, however, required to achieve the rate-plateau condition at saturation was much lower in the presence of TiO_2. The enhanced activities at low CGIS loadings observed in the presence of TiO_2 were explained by the improved dispersion of the powder suspension and optical path in the photoreactor. This TiO_2 supported photocatalyst lowers the required amount of CGIS, which is beneficial from an economic point of view.

1. Introduction

Visible light driven photocatalytic H_2 production is of great interest from both economic and environmental points of view due to its possible application for converting solar energy into carbon-free chemical fuel via water splitting or by oxidizing cheap and abundant compounds [1,2]. For instance, a vast amount of hydrogen sulfide (H_2S) is contained in many natural gas wells, which requires a new economically viable and environmentally-friendly route to convert it [3]. Photocatalysis of H_2S splitting has tremendous benefits over the conventional Claus process because H_2 can be recovered as an advantageous product at refinery sites [4,5]. The photocatalytic efficiency determines the area of the solar reactor, which is directly correlated with the capital cost of the photocatalytic system. Using solar energy as a sustainable energy source, visible light responsive photocatalysts are essential to make the process economically feasible.

Binary chalcogenide nanocrystals are good candidates for visible light photocatalysts for H_2 evolution from S^{2-} containing solutions. For this purpose, CdS has been widely examined [6–9]. Yan et al. reported unprecedented quantum efficiency (QE) in the visible light region (~90% at 420 nm) [10]. The CdS photocatalyst, however, absorbs a limited portion of visible light, i.e., up to 550 nm. Knowing the required thermodynamics of H_2S splitting, i.e., 0.17 eV at standard temperature and pressure, extended visible-light utilization must be considered. The theoretical maximum rate of H_2 production per hour (at 100% QE) for the photocatalyst varies from 0.045 m^3–H_2 m^{-2} (absorption edge of 550 nm) to 0.114 m^3–H_2 m^{-2} (absorption edge of 800 nm). It is therefore challenging to reduce the bandgap while maintaining high QE, although the thermodynamic driving force for redox reactions decreases at narrower bandgaps.

In this context, Kudo and co-workers reported new approaches for bandgap engineering by preparing ternary and quaternary metal sulfide photocatalysts [11,12]. Unlike binary chalcogenide, these nanocrystals have high flexibility for tuning the band

* Corresponding author at: Division of Physical Sciences and Engineering, KAUST Catalysis Center (KCC), King Abdullah University of Science and Technology (KAUST), Thuwal 23955-6900, Saudi Arabia.
** Corresponding author at: Department of Chemistry, Faculty of Science, Sohag University, Sohag 82524, Egypt.
E-mail addresses: kandiel@science.sohag.edu.eg (T.A. Kandiel), kazuhiro.takanabe@kaust.edu.sa (K. Takanabe).

http://dx.doi.org/10.1016/j.apcatb.2015.11.036
0926-3373/

gap without relying on toxic elements [13]. For instance, we prepared $CuGa_2In_3S_8$ nanocrystals that can absorb light up to 700 nm using a facile hot injection method [14]. In this paper, copper–gallium–indium–sulfide (CGIS) nanocrystals with different stoichiometry, i.e., $CuGa_xIn_{5-x}S_8$, where $x = 0–5$, were synthesized and investigated for visible light driven H_2 evolution from aqueous solutions that contain sulfide/sulfite ions. With 1.0 wt.% Ru as co-catalyst, the H_2 evolution rate over $CuGa_2In_3S_8$ had the highest activity. By depositing CGIS nanocrystals on TiO_2 via a unique solvent-induced method, enhanced photocatalytic H_2 evolution activities were observed at low CGIS loadings. This enhancement was due to the synergistic effect between CGIS and TiO_2 or more likely to the improved dispersion and optical properties.

2. Experimental

2.1. Preparation of copper–gallium–indium–sulfide (CGIS) nanocrystals

The $CuGa_xIn_{5-x}S_8$ nanocrystals, where $x = 0–5$, were prepared by a hot-injection method, as previously reported, with modification [14]. Briefly, trace metals of copper(II) acetylacetonate, gallium(III) acetylacetonate, and indium(III) acetylacetonate with the desired ratio were dissolved in 15 mL of oleylamine (70%, Aldrich, technical grade) in a four-necked, round-bottomed flask and stirred at RT for 30 min under an Ar atmosphere. The solution was then heated to 120 °C and maintained at this temperature for 1 h to remove water. The temperature was increased to 150 °C, and 1-dodecanethiol (Sigma–Aldrich) was injected rapidly into the solution under an Ar atmosphere with continuous stirring. The temperature of the solution was maintained at 150 °C for 30 min before it was increased gradually to 285 °C over a period of 30 min. After 24 h, the mixture was cooled, and the nanocrystals were isolated by centrifugation and washed thoroughly with ethanol/hexane (50% v/v). The particles were then dried in a vacuum oven at 45 °C.

2.2. Deposition of CGIS onto the TiO_2 surface

The desired amount of CGIS was dispersed in toluene, followed by the addition of 0.5 g of TiO_2 P25 and sonication for 5 min. The resulting suspension was continuously stirred for 5 h, followed by the addition of 200 mL of ethanol. Then, the CGIS-modified TiO_2 was separated by centrifuge and washed with ethanol three times. The obtained materials were dried at 40 °C in a vacuum oven at 45 °C and were denoted as x-CGIS/TiO_2, where x is the wt.% of CGIS, $x = 1$, 5, 10, 25, 50, and 75 wt.%.

2.2.1. Characterization

Diffuse reflectance spectroscopy (DRS) was performed with a JASCO (V-670) spectrophotometer equipped with a 60 mmØ integrating sphere. A USRS-99-010 labsphere was employed as a reflectance standard. The XRD patterns of the Cu–Ga–In–S nanocrystals were collected on a Bruker D8 Advance diffractometer (DMAX 2500) operating with a CuKα energy source at 40 kV and 40 mA. High-resolution transmission electron microscopy (HRTEM) was performed at 300 kV on a TITAN G2 80–300 ST from FEI. Photoluminescence (PL) spectra were measured using a Fluoromax-4 spectrofluorometer (HORIBA Scientific). XPS analysis was performed by using an AMICUS/ESCA 3400 KRATOS instrument equipped with Mg anodes at 12 kV and 10 mA. A prominent maximum peak of C1s at 284.5 eV was taken as the reference to calibrate the XPS spectra.

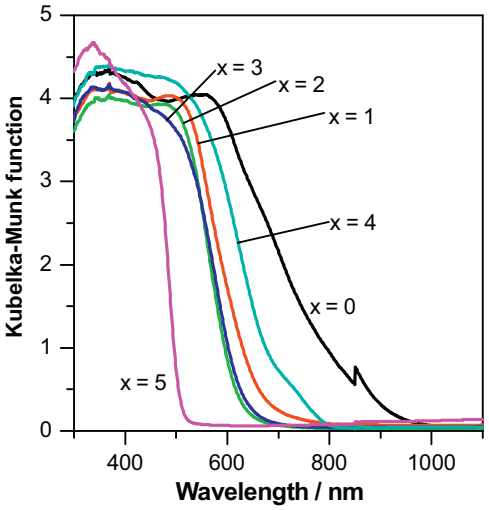

Fig. 1. Diffuse reflectance spectra of $CuGa_xIn_{5-x}S_8$ nanocrystals, where $x = 0–5$.

2.3. Photocatalytic test

The photocatalytic H_2 evolution assessment of the prepared photocatalysts was performed with a Pyrex top-irradiation reaction vessel connected to a glass closed-gas circulation system and a gas chromatograph (Shimadzu 8A). In a typical run, the photocatalyst powder (0.025 g) was dispersed in Na_2S/Na_2SO_3 aqueous solution (25 mL) by sonication. The suspension was poured into the photoreactor, and the desired amount of co-catalyst (i.e., Ru as $RuCl_3{\cdot}xH_2O$ (Ru 38–40%) aqueous solutions) was added. The photoreactor was then sealed and connected to the circulation system. After the photoreactor was evacuated and Ar was introduced several times, the photoreactor was irradiated using a 300 W Xe arc lamp adapted with a wide band-pass filter (MAX-303, Asahai Spectra, 385–740 nm) or narrow band-pass filters. The photon distribution of the band-pass filters was measured using a spectroradiometer (EKO, LS-100) and is presented in Fig. S1. The apparent quantum efficiency (AQE) under white and monochromatic light was calculated as the rate of H_2 evolution ($\mu mol\,h^{-1}$) multiplied by two, divided by the incident photon flux and the illuminated area.

3. Results and discussion

CGIS nanocrystals with different Ga/In ratios, i.e., $CuGa_xIn_{5-x}S_8$, where $x = 0–5$, were synthesized and investigated for photocatalytic H_2 production. Fig. 1 displays the diffuse reflectance spectra of the prepared CGIS nanocrystals with different compositions. The spectra are consistent with the observed color change of the isolated powders with increasing gallium content, going from black for $CuIn_5S_8$ to yellow for $CuGa_5S_8$. Direct determination of the bandgap from the absorbance onset indicates that $CuIn_5S_8$, where $x = 0$, and $CuGa_5S_8$, where $x = 5$, exhibit bandgap values of 1.4 and 2.4 eV, respectively, consistent with the reported bandgap values for stoichiometric $CuInS_2$ and $CuGaS_2$, respectively [15,16]. By controlling the gallium content in the CGIS nanocrystals, the bandgap of the prepared materials can be tuned, as shown in Fig. 1. From the XRD patterns presented in Fig. 2, $CuGa_xIn_{5-x}S_8$, nanocrystals where $x = 1$ and 2, exhibit four prominent peaks at $2\theta = 21.5$, 27.5, 47.6, and 56.2. These peaks are in good agreement with the structure for the $AgGa_2In_3S_8$ reference pattern (PDF 01-070-8366), indicating that they have a layered structure with hexagonal crystal packing [17]. For $CuGa_xIn_{5-x}S_8$ nanocrystals, where $x = 3$, major diffraction peaks for CGIS nanocrystals are observed at 2θ values of 28.9, 56.5, and

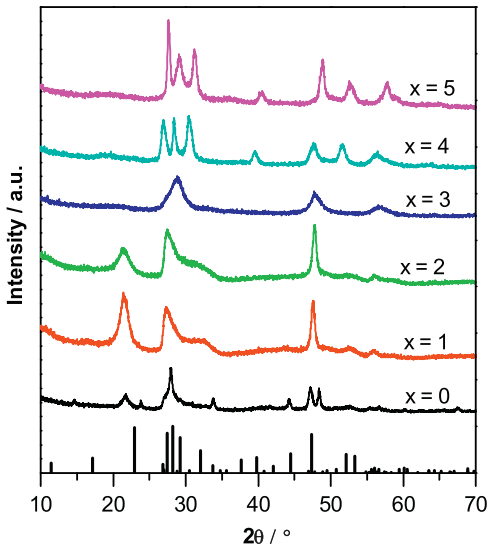

Fig. 2. XRD patterns of $CuGa_xIn_{5-x}S_8$ nanocrystals, where $x = 0–5$.

47.8, indicating the formation of CGIS nanocrystals with zincblende structure [18], whereas at higher gallium content, i.e., where $x = 4$ and 5, the XRD patterns of the CGIS nanocrystals showed major diffraction peaks at 2θ values of 27.6, 29.2, 31.2, 40.4, 48.8, 52.6, and 57.8, with peak positions well-matched with the powder diffraction data reported for the wurtzite structure [19,20].

Table 1
Rates (R_{H2}) and AQE of photocatalytic H_2 evolution from 0.05 mol L^{-1} sodium sulfide/0.3 mol L^{-1} sodium sulfite aqueous solutions over 1.0 wt.% Ru-loaded $CuGa_xIn_{5-x}S_8$ photocatalysts under white light irradiation (photon flux = 1.19×10^3 μmol cm^{-2} h^{-1}).

x in $CuGa_xIn_{5-x}S_8$	R_{H2} (μmol h^{-1})	AQE (%)
0	2.3	0.38
1	19.8	3.32
2	50.6	8.48
2.5	22.8	3.82
3	16.7	2.80
4	28.5	4.78
4.5	10.5	1.76
5	3.2	0.54

To investigate the correlation between light harvesting competency and photocatalytic activity, the rates and AQE of photocatalytic H_2 evolution over 1.0 wt.% Ru-loaded CGIS nanocrystals were measured under visible light illumination and are presented in Table 1. The CGIS nanocrystals with $CuGa_2In_3S_8$ stoichiometry showed the highest activity; however, these nanocrystals absorb a comparable or even lesser amount of photons than CGIS nanocrystals with $x = 0$, 1, and 4 as can be concluded from the diffuse reflectance spectra presented in Fig. 1, assuming that the nanocrystals scatter light with the same ratio. By comparing the photocatalytic activities and the corresponding structures, it can be concluded that the CGIS with layered structure exhibits the highest activity. Many photocatalysts with a layered structured have been reported, and this anisotropic crystal structure and associ-

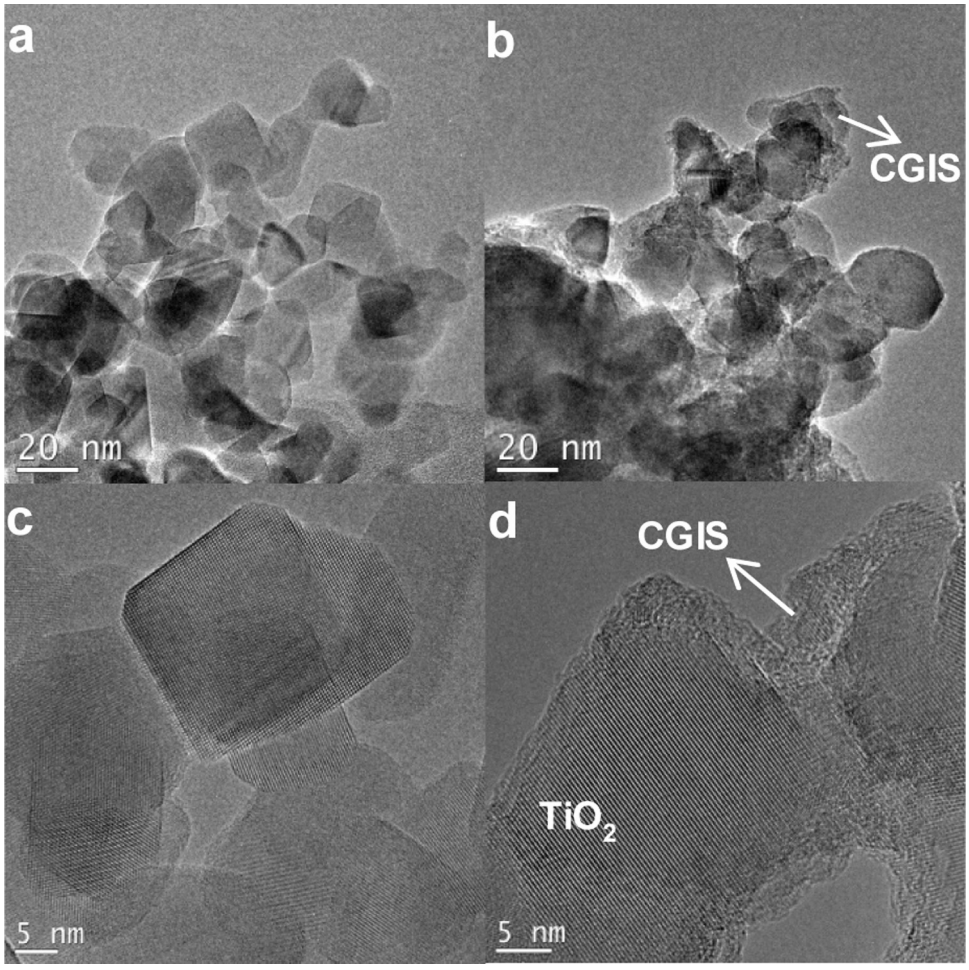

Fig. 3. TEM images of bare TiO_2 p25 (a and c) and $CuGa_2In_5S_8$ deposited onto TiO_2P25 (b and d) at low and high magnifications.

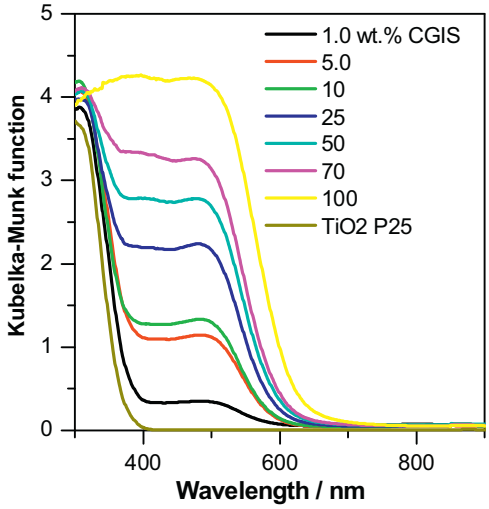

Fig. 4. Diffuse reflectance spectra (DRS) of $CuGa_2In_3S_8$ nanocrystals deposited onto TiO_2 with different weight percentages. For comparison, DRS of bare CGIS and bare TiO_2 P25 are also presented.

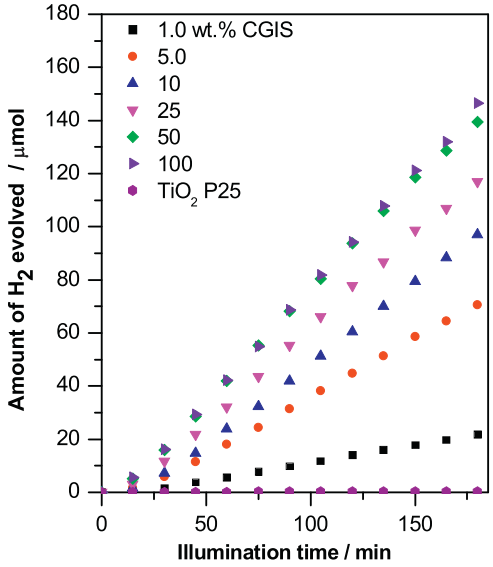

Fig. 5. Time-course of the photocatalytic H_2 evolution over 1.0 wt.% Ru-loaded $CuGa_2In_3S_8$ nanocrystals deposited onto TiO_2. For comparison, bare TiO_2 and bare CGIS are also presented.

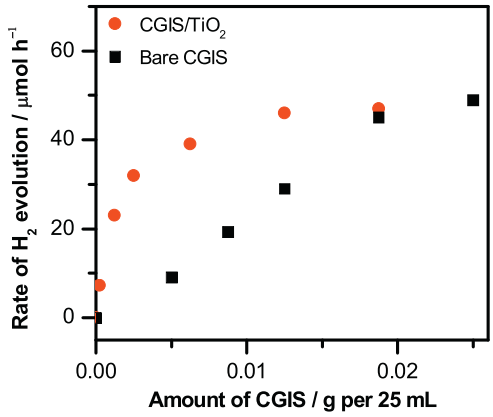

Fig. 6. Effect of the amount of CGIS nanocrystals on the rate of H_2 evolution (■) bare and (●) deposited onto the TiO_2 surface.

ated distinctive charge mobility for electron and hole along with different crystal orientation had positive effects on effective charge separation and resultant photocatalytic activity [11]. The interlayer space is even proposed to act as an active sites for the photocatalytic process [21].

It is desirable to enhance the photocatalytic activity while reducing photocatalyst loading. Thus, the deposition of the most active CGIS nanocrystals, i.e., $CuGa_2In_3S_8$, onto the TiO_2 surface was investigated. The loading was performed using a facile and simple method based on the fact that the as-prepared CGIS nanocrystals are decorated with 1-dodecanethiol and/or oleylamine and thus can be readily dispersed in nonpolar solvents, such as toluene. The dispersion of CGIS nanocrystals in toluene followed by the addition of TiO_2 accompanied by the addition of a polar solvent, such as ethanol, induces the deposition of CGIS nanocrystals onto the surface of TiO_2, as confirmed by the TEM analysis (see Fig. 3). By comparing the TEM images of bare (images a and c) and CGIS deposited on TiO_2 P25 (images b and d), the deposition of CGIS onto the TiO_2 surface can be confirmed. The existence of the CGIS nanocrystals was confirmed by the EDS analysis, as shown in Fig. S2. The optical properties of the CGIS/TiO_2 photocatalysts, where the weight percentages of CGIS were 1.0, 5.0, 10, 25, 50, and 75, were also measured and are presented in Fig. 4. For comparison, the optical properties of bare CGIS and TiO_2 P25 were also measured and presented in Fig. 4. The results indicated that the absorbance of the CGIS/TiO_2 materials in the visible light range increases with increasing the CGIS loadings, indicating the successful loading of the CGIS nanocrystals.

Fig. 5 shows the time courses of the photocatalytic H_2 evolution from 0.05 mol L^{-1} sodium sulfide/0.3 mol L^{-1} sodium sulfite aqueous solutions employing CGIS/TiO_2 photocatalysts. The loading of the photocatalyst, including TiO_2, was kept constant at 1.0 g L^{-1}. The rate of the H_2 evolution increased with increasing the amount of CGIS deposited onto the surface of TiO_2, indicating that the CGIS material is the photoactive part. This behavior agrees well with the light absorbance characteristics presented in Fig. 4. For comparison, the time courses of the photocatalytic H_2 evolution over bare TiO_2 and bare CGIS are also measured and presented in Fig. 5. TiO_2 is a wide bandgap semiconductor and does not absorb visible light, thus exhibiting negligible activity, as shown in Fig. 5. Because TiO_2 does not contribute to photocatalytic H_2 evolution under the current conditions, it is worth normalizing the amount of evolved H_2 per the amount of CGIS nanocrystals supported on the TiO_2 surfaces to compare the activities of bare CGIS nanocrystals and CGIS nanocrystals deposited on TiO_2. However, the amount of evolved H_2 does not linearly depend on the amount of the photocatalyst employed; thus, the normalization of the amount of evolved H_2 per the amount of used photocatalyst results in improved rate per gram of photocatalyst. To avoid overestimation, a comparison should be performed in the range where the photocatalytic H_2 evolution rate increases with an increasing amount of photocatalyst, i.e., before saturation. To define this range, the effect of the bare CGIS photocatalyst loading on the H_2 evolution rate was investigated and is present in Fig. 6. The results showed that under the current conditions, the rate of H_2 evolution increases almost linearly as a function of photocatalyst loading up to 25 mg per 25 mL (i.e., 1.0 g L^{-1}); then, the rate levels off and remains almost constant.

The rates of H_2 evolution over CGIS/TiO_2 photocatalysts were plotted against the amount of CGIS supported on TiO_2 and are presented in Fig. 6. Fig. 6 shows that the amount of the CGIS to reach the plateau of H_2 evolution rate is reduced to half when using TiO_2 as a support; the rate of H_2 evolution is comparable to that observed over bare CGIS when the amount is doubled. The enhancement is more substantial at lower CGIS loadings on TiO_2. The enhanced photocatalytic activity observed when using CGIS/TiO_2 photocatalysts

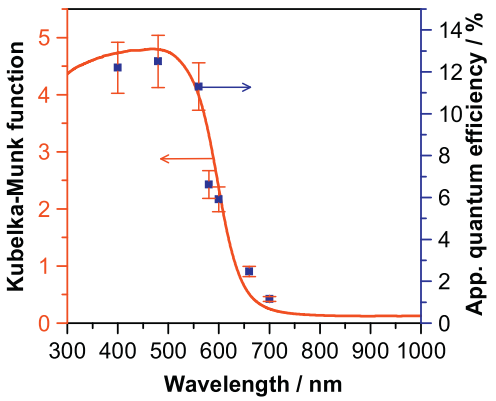

Fig. 7. Action spectrum of H_2 evolution over 50 wt.%-CGIS/TiO_2. Conditions: Na_2S (0.05 mol L^{-1})/Na_2SO_3 (0.3 mol L^{-1}) aqueous solution, 1.0 wt.% Ru co-catalyst. The diffuse reflectance spectrum of CGIS nanocrystals is included for comparison.

compared bare CGIS nanocrystals can be explained by the enhanced electron transfer between CGIS and TiO_2, the improved dispersion of the photocatalyst powder in the solution and the improved optical properties in the presence of TiO_2. From a thermodynamic point of view, the conduction band edge of TiO_2 is positioned at −0.2 V vs. RHE [22], whereas the conduction band edge of CGIS is positioned at −0.6 vs. RHE at pH 12 [14]. Thus, the conduction band edge of CGIS is approximately 0.4 eV more negative than that of TiO_2, indicating potential electron transfer from CGIS to TiO_2 without back electron transfer, which may lead to better charge carrier separation and thus to an increase in photocatalytic activity, as is commonly encountered in the case of anatase/rutile mixtures [23–25] and CdS-loaded TiO_2 [26,27]. However, it is reasonable to consider that, in our experiment, the improved charge separation is unlikely the reason for this finding because the rate at the plateau in terms of photocatalyst amount (saturation) gave similar values for bare and supported CGIS photocatalysts. Therefore, electron transfer is not the cause of this rate enhancement. The photoluminescence (PL) spectra of bare CGIS, CGIS/TiO_2 and TiO_2 P25 failed to provide evidence of charge transfer, as they show negligible differences (see Fig. S3). The TiO_2 nanoparticles scatter light, which influences the total path of the visible light in the photoreactor. To further rationalize the benefit of the deposition of CGIS nanocrystals onto the TiO_2 surface using the solvent-induced deposition method, the CGIS nanocrystals were tested together with TiO_2 by physical mixing. The photocatalytic H_2 evolution measurements indicated that the rate of photocatalytic H_2 evolution using CGIS-TiO_2 photocatalyst via physical mixing was not significantly improved (see Fig. S4), excluding a strong contribution of light management in the photoreactor in the presence of TiO_2. Therefore, the dispersion of CGIS in toluene followed by the addition of ethanol creates a better dispersion of the CGIS nanocrystals onto the TiO_2 particles, as evident from the TEM images (Fig. 3). For comparison, the CGIS was supported on SiO_2 nanoparticles (~20 nm spherical powder) by the solvent-induced deposition method. No prominent improvement was achieved with SiO_2, compared with TiO_2 (see Fig. S4), which may suggest that the synergistic effect between CGIS nanocrystals closely located on TiO_2 contributes to the improved photocatalytic H_2 evolution activity. It may be a specific interaction between CGIS and TiO_2, but further examination to determine the exact cause is required. It is worth mentioning that Ru sulfide precipitates were formed when Ru precursor was added to the Na_2S/Na_2SO_3 aqueous solution. XPS measurements confirmed the formation of Ru*Sx* (see Fig. S5). As it can be seen in Fig. 3, CGIS completely covers the surface of TiO_2 and thus the Ru sulfide species are more likely deposited on the CGIS outer surface and acted as a co-catalyst, consistent with the recent literature [28], although we failed to identify Ru species in TEM images probably due to the low contrast between Ru and CGIS material. Accordingly, it was not possible to prove synergistic effect between CGIS and TiO_2 by defining the location of the deposited Ru species. The AQE of H_2 evolution over 50 wt.% CGIS loaded TiO_2 was measured under semi-monochromatic irradiation using band-pass filters and is presented in Fig. 7. For comparison, the diffuse reflectance spectrum of bare CGIS is also shown in Fig. 7. The onset of the action spectrum is in good agreement with the diffuse reflectance spectrum, which indicates that photocatalytic H_2 evolution proceeds through the excitation of the CGIS nanocrystal band gap.

4. Conclusions

In conclusion, copper–gallium–indium–sulfide (CGIS) nanocrystals with different Ga/In ratios were synthesized and investigated for visible-light-driven H_2 evolution from aqueous solutions that contain sulfide/sulfite ions. The $Cu_2Ga_2In_3S_8$ showed the highest activity among the different prepared CGIS nanocrystals. A unique, solvent-induced deposition method for depositing CGIS nanocrystals onto a TiO_2 surface was developed. The as-prepared CGIS nanocrystals are decorated with 1-dodecanethiol and/or oleylamine and thus can be readily dispersed in nonpolar solvents, such as toluene. The dispersion of CGIS and TiO_2 in toluene followed by the addition of polar solvent, such as ethanol, induces the deposition of CGIS onto the surface of TiO_2. The CGIS nanocrystals supported on TiO_2 showed an enhanced rate based on the photocatalyst amount when utilizing a small quantity of the CGIS materials photocatalyst. This enhancement is explained by the improved dispersion and optical properties of the photocatalyst materials in the photoreactor. For large scale application, it is desirable from the economic point of view to achieve H_2 evolution rates with reduced photocatalyst amounts.

Acknowledgments

Funding for this work was provided by Saudi Aramco under contact 6600024505/01. The research reported in this work was supported by the King Abdullah University of Science and Technology. T.A.K. thanks the Chemistry Department, Faculty of Science at Sohag University for granting him a leave of absence.

Appendix A. Supplementary data

Supplementary data associated with this article can be found, in the online version, at http://dx.doi.org/10.1016/j.apcatb.2015.11.036.

References

[1] K. Maeda, K. Teramura, D. Lu, T. Takata, N. Saito, Y. Inoue, K. Domen, Nature 440 (2006) 295.
[2] G. Ma, H. Yan, J. Shi, X. Zong, Z. Lei, C. Li, J. Catal. 260 (2008) 134–140.
[3] J.H. Gary, G.E. Handwerk, Petroleum Refining Technology and Economics, Fourth ed., Marcel Dekker Inc, New York, Basel, 2005.
[4] I.A. Gargurevich, Ind. Eng. Chem. Res. 44 (2005) 7706–7729.
[5] N.S. Chaudhari, A.P. Bhirud, R.S. Sonawane, L.K. Nikam, S.S. Warule, V.H. Rane, B.B. Kale, Green Chem. 13 (2011) 2500–2506.
[6] H. Park, W. Choi, M.R. Hoffmann, J. Mater. Chem. 18 (2008) 2379–2385.
[7] J. Yu, Y. Yu, P. Zhou, W. Xiao, B. Cheng, Appl. Catal. B Environ. 156–157 (2014) 184–191.
[8] Q. Xiang, B. Cheng, J. Yu, Appl. Catal. B Environ. 138–139 (2013) 299–303.
[9] W. Yu, T. Isimjan, S.D. Gobbo, D.H. Anjum, S. Abdel-Azeim, L. Cavallo, A.T. Garcia-Esparza, K. Domen, W. Xu, K. Takanabe, ChemSusChem 7 (2014) 2575–2583.
[10] H. Yan, J. Yang, G. Ma, G. Wu, X. Zong, Z. Lei, J. Shi, C. Li, J. Catal. 266 (2009) 165–168.
[11] H. Kaga, K. Saito, A. Kudo, Chem. Commun. 46 (2010) 3779–3781.
[12] I. Tsuji, Y. Shimodaira, H. Kato, H. Kobayashi, A. Kudo, Chem. Mater. 22 (2010) 1402–1409.

[13] D. Aldakov, A. Lefrançois, P. Reiss, J. Mater. Chem. C 1 (2013) 3756–3776.
[14] T.A. Kandiel, D.H. Anjum, K. Takanabe, ChemSusChem 7 (2014) 3112–3121.
[15] J. Chang, E.R. Waclawik, CrystEngComm 15 (2013) 5612–5619.
[16] Q. Li, C. Zou, L. Zhai, J. Shen, L. Zhang, H. Yu, Y. Yang, X.a. Chen, S. Huang, J. Alloys Compd. 567 (2013) 127–133.
[17] H. Haeuseler, E. Elitok, A. Memo, R. Arzani, Z. Anorg, Allg. Chem. 627 (2001) 1204–1208.
[18] W. Yue, S. Han, R. Peng, W. Shen, H. Geng, F. Wu, S. Tao, M. Wang, J. Mater. Chem. 20 (2010) 7570–7578.
[19] T.A. Kandiel, D.H. Anjum, P. Sautet, T. Le Bahers, K. Takanabe, J. Mater. Chem. A 3 (2015).
[20] M.D. Regulacio, C. Ye, S.H. Lim, Y. Zheng, Q.-H. Xu, M.-Y. Han, CrystEngComm 15 (2013) 5214–5217.
[21] A. Kudo, K. Sayama, A. Tanaka, K. Asakura, K. Domen, K. Maruya, T. Onishi, J. Catal. 120 (1989) 337–352.
[22] G. Rothenberger, D. Fitzmaurice, M. Gratzel, J. Phys. Chem. 96 (1992) 5983–5986.
[23] T.A. Kandiel, R. Dillert, A. Feldhoff, D.W. Bahnemann, J. Phys. Chem. C 114 (2010) 4909–4915.
[24] T. Kawahara, Y. Konishi, H. Tada, N. Tohge, J. Nishii, S. Ito, Angew. Chem. Int. Ed. 41 (2002) 2811–2813.
[25] O.O. Prieto-Mahaney, N. Murakami, R. Abe, B. Ohtani, Chem. Lett. 38 (2009) 238–239.
[26] K. Ogisu, K. Takanabe, D. Lu, M. Saruyama, T. Ikeda, M. Kanehara, T. Teranishi, K. Domen, Bull. Chem. Soc. Jpn. 82 (2009) 528–535.
[27] Z. Chen, Y.-J. Xu, ACS Appl. Mater. Interfaces 5 (2013) 13353–13363.
[28] M. Tabata, K. Maeda, T. Ishihara, T. Minegishi, T. Takata, K. Domen, J. Phys. Chem. C 114 (2010) 11215–11220.